Relaxation Shortcuts through Boundary Coupling

Gianluca Teza, Ran Yaacoby, and Oren Raz*
Department of Physics of Complex Systems, Weizmann Institute of Science, Rehovot 7610001, Israel

(Received 23 December 2021; revised 6 July 2022; accepted 17 May 2023; published 6 July 2023)

When a hot system cools down faster than an equivalent cold one, it exhibits the Mpemba effect (ME). This counterintuitive phenomenon was observed in several systems including water, magnetic alloys, and polymers. In most experiments the system is coupled to the bath through its boundaries, but all theories so far assumed bulk coupling. Here we build a general framework to characterize anomalous relaxations through boundary coupling, and present two emblematic setups: a diffusing particle and an Ising antiferromagnet. In the latter, we show that the ME can survive even arbitrarily weak couplings.

DOI: 10.1103/PhysRevLett.131.017101

When coupled to a thermal bath, most systems relax toward equilibrium. While the equilibrium distribution is only a function of the system's Hamiltonian and temperature, the precise details of the relaxation are determined by many factors, including the intrinsic properties of the specific system, its initial condition, the bath's properties, and the exact nature of the coupling between the system and the bath.

In the weak coupling limit, when the rate of heat exchange with the thermal environment is much slower than the energy relaxation within the system, it is generally expected that a macroscopic system initiated at equilibrium with temperature T_0 relaxes *quasistatically* toward the bath temperature T_b, such that the system is in equilibrium for some temperature throughout the relaxation. This is a consequence of the self-thermalization generated by the energy diffusion within the system being much faster than the rate of heat exchange with the thermal bath. In strong couplings, however, the self-thermalization process that equilibrates the system is not fast enough, and the energy exchange with the environment drives the system into a relaxation trajectory that can reach far from any equilibrium distributions. These far from equilibrium relaxation trajectories can be counterintuitive, and show interesting phenomena unexpected near equilibrium [1–5]. An important example is the Mpemba effect (ME) [6,7], where a hot system cools faster than an initially cold one when quenching both to an even colder bath. The ME was observed experimentally in a variety of setups, including water [8], magnetic alloys [9], polymers [10], clathrate hydrates [11], and very recently in small size systems like colloids diffusing in a potential [12–14]. It was also observed in a variety of numerical and theoretical models for water molecules [15–20], driven granular gases [21–26], inertial suspensions [27–29], gas of viscoelastic particles [30], diffusing in a potential [2,31–34], and classical as well as quantum spin models [35–42].

The theoretical models proposed so far to explain anomalous relaxation phenomena as the ME used the simplifying assumption that all the relevant degrees of freedom (e.g., all spins or molecules) are directly coupled to the thermal bath. However, in all relevant experiments so far, only a small set out of the relevant degrees of freedom are coupled to the bath. For example, in water, clathrate hydrates, and polymers, internal collisions between the molecules conserve energy, and the system exchanges heat with the bath only through boundary collisions [43,44]. Even in the case of colloidal systems [12,13], the colloid interacts with the liquid around them, but the liquid exchanges heat with the bath only through its boundaries.

In this Letter, we construct a general theoretical framework for boundary coupling with the bath, and use it to demonstrate the existence of the ME even in such systems. We consider two types of systems: (i) systems where the relevant degrees of freedom (d.o.f.) interact with a "local bath" composed of other degrees of freedom, in which case, the local temperature profile changes with a characteristic timescale, defining an interplay with the dynamics of the relevant d.o.f. which will determine the possibility of observing ME and other anomalous relaxation phenomena, and (ii) systems where the same d.o.f. both play the role of the relaxation and serve as a local bath, in which case, the situation is quite different: in these scenarios the ME is possible even in the arbitrarily weak coupling limit.

Diffusing particle.—A prominent example for the first kind of system is a Brownian particle diffusing in a confining potential. When the system is quenched to some temperature, the fluid in which the particle is diffusing does not change its local temperature instantaneously and uniformly. Rather, its boundaries are coupled to a thermal bath, and the temperature profile changes according to some internal dynamics. If this dynamics is much faster than the particle diffusion, the liquid reaches its uniform temperature before the distribution of the relevant d.o.f. (i.e., the position) changes in any way. This case coincides with the

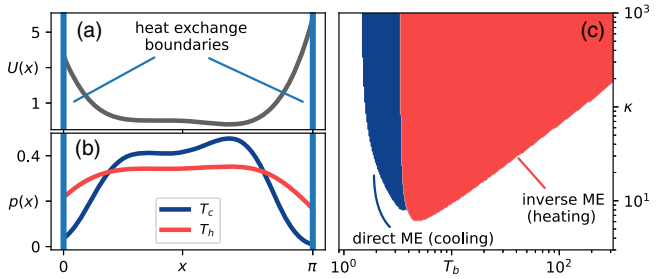

FIG. 1. (a) Double-well potential $U(x)$ similar to that used in colloidal experimental setups (see Refs. [12,13]). (b) Examples of Boltzmann distributions at cold and hot bath temperatures for which the direct (cooling) and inverse (heating) ME exist. (c) Mpemba phase diagram as a function of the bath temperature T_b and thermal diffusivity κ.

common assumption of instantaneous uniform quench in the temperature. In the opposite limit, the equilibration temperature profile is much slower than the diffusion, and the position of the particle follows the steady-state distribution associated with the instantaneous temperature profile. Anomalous relaxations can therefore exist only in the local bath temperature profile, which is assumed not to be the case. This implies that a certain "critical coupling," determining the possibility of observing anomalous relaxation phenomena, exists.

To demonstrate this case, we use the Brownian particle in a potential used to demonstrate experimentally the inverse [13] and strong [12] Mpemba effects [see Fig. 1(a)]. However, instead of using a uniform instantaneous quench of the temperature at all position as in Refs. [12,13], here the system is coupled to the thermal bath only from its boundaries [Fig. 1(a)]. We assume that the water's temperature profile follows the heat equation $\partial_t T(x,t) = \kappa \partial_x^2 T(x,t)$ with initial condition given by the spatially uniform initial temperature $T(x,t=0) = T_0$ and thermal diffusivity κ. The probability density $p(x,t)$ of finding the particle in position x at some time t evolves according to the Fokker-Plank equation [45]:

$$\begin{aligned}\partial_t p(x,t) &= -\mu\partial_x([\partial_x U(x)]p(x,t)) + \mu\partial_x^2(T(x,t)p(x,t)) \\ &\equiv \mathcal{L}(t)p(x,t), \end{aligned} \tag{1}$$

where $U(x)$ is the potential and μ is the mobility of the Brownian particle. The Fokker-Plank operator is time dependent, but in the long time limit $T(x) \to T_b$, implying $\mathcal{L}(t) \to \mathcal{L}_{T_b}$ which ensures convergence to the Boltzmann equilibrium $\pi_{T_b}(x) \propto e^{-U(x)/T_b}$ (we set $k_b = 1$). The eigenfunctions of $\mathcal{L}_{T_b}$, solving $\mathcal{L}_{T_b} v_i(x,T_b) = \lambda_i v_i(x,T_b)$ with $0 = \lambda_1 > \lambda_2 \geq \lambda_3 \geq \ldots$, form a complete basis; therefore,

$$p(x,t) = \pi_{T_b}(x) + \sum_{i>1} a_i(T_0,T_b,t) e^{\lambda_i(T_b)t} v_i(x,T_b), \tag{2}$$

where $a_i(t)$ is a coefficient retaining information on the initial conditions of the system, as well as the temperature profile.

In the limit of an instantaneous quench, a_i are time independent, and a_2 encodes the existence of the ME, as was used in [12,13]: a nonmonotonic dependence in T_0 implies the existence of a relaxation shortcut when quenching the system to T_b, which can be exponentially faster if $a_2 = 0$ for some initial condition (a *strong* ME). However, when the timescale of the quench is comparable to that of the diffusing particle, one cannot rely on the same analysis as in Refs. [12,13], as a_2 has a nonexponential time dependence due to the time-dependent temperature profile. In the last stages of the relaxation, one can nevertheless approximate the difference from equilibrium $\Delta p(x,t) = p(x,t) - \pi_{T_b}(x) \simeq a(t)v_2(x)$ for some $a(t)$ decaying exponentially fast. Identifying a sign change in $a(t)$ is therefore enough to ensure the existence of a strong ME. Formally, this can be done through the Mpemba parity index [40]

$$I^{\pm}(t,T_b) = \mathrm{sgn} \int dx \Delta p^{\pm}(x,t) \Delta p^{\pm \delta T}(x,t), \tag{3}$$

where the differences $\Delta p^{\pm}$ refer to quenches to T_b starting from initial temperatures $T_0 = \{+\infty, 0\}$, while $\Delta p^{\pm\delta T}$ to quenches starting from $T_0 = T_b \pm \delta T$, for some $\delta T > 0$. A negative sign of I^+ (I^-) in the long time limit implies that for some $T > T_b$ ($T < T_b$) the coefficient $a_2 \equiv 0$, ensuring the existence of a strong direct (inverse) ME. For the given potential $U(x)$ [Fig. 1(a)], and for each set of T_b and κ, it is possible to evaluate numerically $I^{\pm}$ as demonstrated in Fig. 1(c). As expected, for a given value of T_b, there exists a critical value of κ below which the ME cannot be observed.

Boundary d.o.f. coupling.—Let us next discuss a different type of system, in which all the d.o.f. are modeled, but only the boundary d.o.f. can exchange heat with the environment. For simplicity, we use a discrete state system with probability distribution $\vec{p}(t)$ where the component $p_i(t)$ is the probability to be in a microstate i at a given time t. $\vec{p}(t)$ evolves in time according to a Markovian master equation

$$\partial_t \vec{p}(t) = \mathbf{W}(T_b)\vec{p}(t), \tag{4}$$

where the rate matrix $\mathbf{W}$ generalizes the Fokker-Plank operator $\mathcal{L}$ and encodes the specific model. The off diagonal terms $\mathbf{W}_{ij}$ are the transition rates from state j to state i, while the diagonal term $\mathbf{W}_{ii} = -\sum_{j\neq i} \mathbf{W}_{ji}$ represents the escape rate from the state i. We assume that detailed balance and ergodicity hold, so that regardless of the initial condition the system relaxes toward the Boltzmann distribution $\pi_i(T_b) \propto e^{-E_i/T_b}$ where E_i is the energy of the microstate i. In this case, the relaxation process from equilibrium with an initial temperature T_0 is a discrete analog of Eq. (2), allowing us to straightforwardly

characterize the ME through the coefficient a_2 [1]. For simplicity, in what follows, we do not distinguish between different types of the ME.

To model the common scenario where heat can be transferred only through d.o.f. sitting on the boundaries, we first distinguish between "boundary transitions" of boundary d.o.f. that can exchange heat with the bath, and "bulk transitions" in which no energy is exchanged with the bath and they can only happen between same-energy states. Bulk transitions serve as a *self-thermalization* (ST) mechanism, whereas the boundary transitions generate *bath coupling* (BC) and enable transitions between different energy shells. This structure can be modeled by

$$\mathbf{W}(\Gamma^{\mathrm{ST}},\Gamma^{\mathrm{BC}}) = \Gamma^{\mathrm{ST}}\mathbf{W}^{\mathrm{ST}} + \Gamma^{\mathrm{BC}}\mathbf{W}^{\mathrm{BC}}. \tag{5}$$

Here $\mathbf{W}^{\mathrm{ST}}$ and $\mathbf{W}^{\mathrm{BC}}$ are normalized rate matrices corresponding to the self-thermalization and boundary coupling transitions respectively, and $\Gamma^{\{\mathrm{ST,BC}\}}$ are coupling constants modulating the rates amplitude. Their ratio, $C = \Gamma^{\mathrm{BC}}/\Gamma^{\mathrm{ST}}$, dictates the coupling strength [46]: in the limit $C \ll 1$ boundary flips occur rarely compared with thermalization flips; hence the system thermalizes quickly after each heat exchange with the bath. In the $C \gg 1$ limit, the boundaries exchange heat much faster than the thermalization, and the diffusion of energy within the system sets the timescale for the relaxation. We refer to the former limit as *weak coupling* and to the latter as *strong coupling*. By construction, $\mathbf{W}^{\mathrm{BC}}$ is generally sparse, and $\mathbf{W}^{\mathrm{ST}}$ contains only transitions between same-energy states, implying a degeneracy of its zeroth eigenvalue equivalent to the number of energy shells.

In the weak coupling limit, a naive perturbation scheme with $C \ll 1$ would not prove useful: for $C = 0$ the matrix $\mathbf{W}$ is reducible, and its zero eigenvalue is highly degenerate, so one cannot apply the standard analysis. Instead, it is constructive in this case to aggregate all the microstates that share the same energy into a single *macrostate* and construct the effective dynamics by summing all the microscopic transitions between them [47,48]. The dynamics is then dictated only by the boundary flips, and the diffusion within each energy shell is assumed to happen instantaneously. Similarly, in the strong coupling limit, microstates can be aggregated into macrostates by combining all the microstates connected by boundary flips. Mathematically, the two aggregation procedures can be done by arranging the states such that $\mathbf{W}^{\mathrm{BC}}$ or $\mathbf{W}^{\mathrm{ST}}$ is block diagonal where each block corresponds to transitions within a macrostate, and coarsening over these blocks.

Ising antiferromagnet.—Let us demonstrate the above construction with a specific example of N Ising spins on a ring, with nearest neighbor antiferromagnet interactions [Fig. 2(a)]. Each spin $\{\sigma_s\}_{s=1\ldots N}$ can either be in a $+1$ or -1 state, giving a total of $M = 2^N$ different microstates,

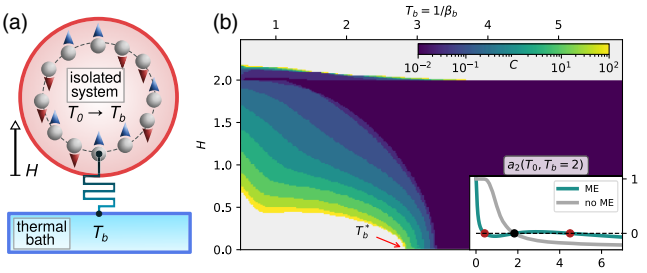

FIG. 2. (a) An antiferromagnet Ising chain, with a single spin coupled to the thermal bath. Transitions are allowed only if energy is conserved, except for flipping the spin coupled to the bath. (b) Minimal coupling strength C (colorbar) for which there exists some type of a ME at the corresponding bath temperature T_b (x axis) and H (y axis). In the white areas there is no ME at any coupling strength. Inset: the ME exists if $a_2(T_0, T_b)$ is nonmonotonic in T_0.

identified by $\vec{\sigma} = (\sigma_1, \ldots, \sigma_N)$. The Hamiltonian of the system is

$$\mathcal{H}(\vec{\sigma}) = -J\sum_s \sigma_s\sigma_{s+1} - H\sum_{s=1}^{N}\sigma_s, \tag{6}$$

where $J < 0$ is the coupling constant, H is an external magnetic field, and $\sigma_{N+1} \equiv \sigma_1$. For simplicity, we set $J = -1$.

As a boundary, we choose a specific spin (say σ_1) to be coupled to the bath. This implies that a general microstate $\vec{\sigma}$ is connected through thermal flips only with a single state $\vec{\sigma}'$ in which the first spin is flipped, $\sigma_1 \to -\sigma_1$, while the remaining spins are unaltered. The transition between two general microstates $\vec{\sigma}^{\{i,j\}}$ is therefore

$$\mathbf{W}^{\mathrm{BC}}_{ij} = \frac{\delta_{\sigma_1^i,-\sigma_1^j}\prod_{s>1}\delta_{\sigma_s^i,\sigma_s^j}}{1 + e^{(\mathcal{H}(\vec{\sigma}^i)-\mathcal{H}(\vec{\sigma}^j))/T_b}} \tag{7}$$

where δ_{ij} is the Kronecker delta, σ_s^i is the s spin in the microstate $\vec{\sigma}^i$, and we used standard Glauber dynamics as the transition weight [49,50], ensuring equilibration to a Boltzmann distribution.

To model bulk transitions we use rates that decay exponentially as $2^{-d_{ij}}$, where $d_{ij} = \sum_s \delta_{\sigma_s^i,-\sigma_s^j}$ is the Hamming distance [51] that counts the number of spins that has to be flipped between the two configurations. Alternative metrics that keep into account space locality (e.g., the generalized Hamming distance [52]) could be implemented. While for weak couplings the specific details of d_{ij} become irrelevant, for strong couplings locality constraints limit the connectivity within an energy shell, effectively enhancing the out-of-equilibrium character of the relaxation process (see the Supplemental Material [53]). We therefore formalize bulk transitions between two states $i \neq j$ as

$$\mathbf{W}_{ij}^{\mathrm{ST}} = \delta_{\mathcal{H}(\vec{\sigma}^i),\mathcal{H}(\vec{\sigma}^j)} 2^{-d_{ij}}. \tag{8}$$

The full transition matrix for the model is built as a linear combination of the two rate matrices as in Eq. (5).

Let us consider the persistence of the ME in this setup. In Fig. 2(b) we plot for each T and H the minimal coupling constant C for which some type of a ME exists in the system, for $N = 10$. The strength of the coupling affects only *quantitatively* the regions where the ME can be observed (the larger C, the larger the area). In particular, for any $|H| \leq 2$ the effect exists for any $T > T_b^*$, highlighted in Fig. 2(b) with a red arrow.

In the weak coupling case ($C \ll 1$), the coarse-grained rate matrix is given by

$$\mathbf{W}_{ij}^{\mathrm{weak}} = \frac{G_{ij}}{\Omega_j} \frac{1}{1 + e^{(E_i - E_j)/T_b}}, \tag{9}$$

where the indices i, j now refer to the energies E_i and E_j, the (symmetric) matrix G_{ij} counts the number of transitions connecting microstates in the two energy shells, and Ω_i is the number of microstates with energy E_i. This coarsening considerably reduces the size of the matrix, allowing one to numerically analyze longer chains assessing the stability of the phase diagram in the thermodynamic limit. The total number of energy shells in this case grows only quadratically as $2 + (N/2)^2$, as opposed to the exponential growth of the number of microstates. As an example, at $N = 50$ [Figs. 3(c) and 3(d)] there are $\sim 10^{15}$ microstates, but only 627 macrostates in the coarse-grained representation. A specific example exhibiting a strong ME in this setup is presented in the Supplemental Material [53].

Extremely strong couplings ($C \gg 1$) can be similarly analyzed. In our model only a single spin is coupled to the bath; therefore the clustering of a N spin chain model results in an effective $N - 1$ long chain with an additional "superposed" spin oscillating infinitely fast between the two ± 1 states. Indicating with i one of the possible 2^{N-1} configurations of the bulk chain, we set $\mathcal{H}_i^{\pm 1}$ to be the Hamiltonians of each of the two possible states in the ith cluster. The two states composing a cluster are not equivalent as in the weak coupling case. To correctly define the transition rates in the coarse-grained model we therefore need to introduce a Glauber weight: $w_j^\sigma = e^{-\mathcal{H}_j^\sigma/T_b}/(e^{-\mathcal{H}_j^{-1}/T_b} + e^{-\mathcal{H}_j^{+1}/T_b})$ with $\sigma = \pm 1$ depending on the microstate from which the original transition occurred. This provides us with

$$\mathbf{W}_{ij}^{\mathrm{strong}} = \sum_{\sigma,\sigma'} w_j^\sigma \delta_{\mathcal{H}_j^\sigma,\mathcal{H}_i^{\sigma'}} 2^{-(d_{ij} + \delta_{\sigma,-\sigma'})} \tag{10}$$

where the Kroneker delta corrects the Hamming distance for the coupled spin. The area in which an effect can be observed is wider [Fig. 3(a)]: a stronger coupling should indeed ease the undertake of anomalous relaxation paths.

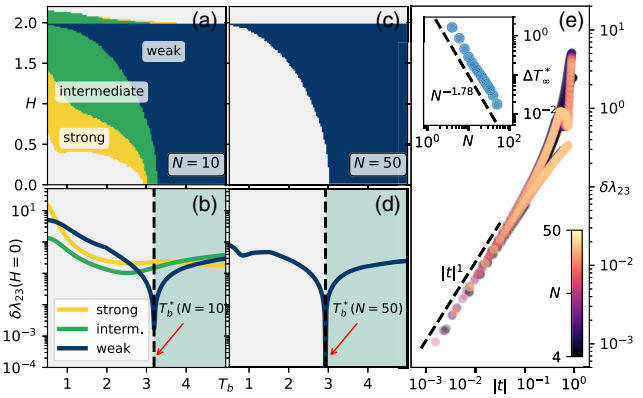

FIG. 3. (a) Comparison of the ME for different coupling strengths ($N = 10$). The strong coupling limit ($C \gg 1$) includes all colored areas, while the intermediate coupling ($C = 1$) is limited to the green and blue ones. Surprisingly, the effect survives the arbitrarily weak coupling limit ($C \ll 1$, blue area). (b) Distance between the second and third eigenvalues $\delta\lambda_{23}$ as a function of T_b for $H = 0$. A crossing of the eigenvalues clearly marks the beginning of the Mpemba region at T_b^* for the weakly coupled model. (c),(d) Phase diagram in the weak coupling limit for $N = 50$. (e) Collapse of $\delta\lambda_{23}$ for different sizes shows a dependence on the rescaled temperature $\propto |t|^1$. In the inset, the distance from the asymptotic $T_b^* \sim 2.91$ scales superlinearly.

In Fig. 3(a) we plot the regions in which some ME can be observed in the limiting coupling setups discussed above, and compare them with the intermediate $C = 1$ case. Surprisingly, the ME can be observed even for $C \ll 1$, demonstrating that the effect survives the limit of arbitrarily weak coupling. This counterintuitive result is related to the discrete nature of the d.o.f. of the system [54]. Indeed, Glauber dynamics [Eq. (7)] allows transitions only among configurations that differ by a single spin flip. This implies that energy shells with a microscopic energy difference (namely $\Delta E \sim 1$ even though $E \sim N$) might still be very far in terms of transitions. As a result, the self-thermalization process has the same characteristic timescale as that of the boundary transitions. Therefore for arbitrarily weak couplings, even in the thermodynamic limit the system is forced to explore out-of-equilibrium configurations that allow the existence of anomalous relaxation effects (i.e., the ME). The colloidal particle setup (Fig. 1) provides a counterexample in which the continuous d.o.f. break such mechanisms, setting a minimal value of the coupling strength below which no ME can be observed.

The boundary coupling setup we introduced offers a straightforward implementation for multiple baths coupling. If the baths are set at different temperatures, the rate matrix no longer abides by detailed balance, driving the system toward a nonequilibrium steady-state (NESS) that does not correspond to any Boltzmann distribution [48,55,56]. Nondominant eigenvalues can be complex

valued, determining the onset of oscillating relaxations [53] where an analogous ME analysis allows one to determine which initial equilibrium conditions relax the fastest (or slowest) to the NESS.

Finally, our analysis highlights a strong connection between the ME and the phenomenon of *eigenvalue crossing* of the transition matrix $\mathbf{W}$ with respect to the bath temperature T_b [57], which was recently connected to a new kind of dynamical phase transitions that further consolidates the parallel between singularities in the dynamics and equilibrium phase transitions [58–60]. In weakly coupled systems, an analysis of $\delta\lambda_{23} = (\lambda_3 - \lambda_2)/\lambda_2$ at $H = 0$ shows how the bath temperature above which the ME can be observed is determined by a crossing at a certain "critical" temperature T_b^*. This corresponds to a singularity in the eigenvector regulating the direction of the slowest relaxation, determining the conditions that allow the existence of the ME [Figs. 3(b) and 3(d)]. Analyses at different sizes show an excellent multiscale collapse [61] on the rescaled temperature $t = (T_b - T_b^*)/T_b^*$ around zero, with a dependence $\delta\lambda_{23} \propto |t|^1$ [Fig. 3(e)]. The critical temperature at finite sizes approaches the asymptotic value $T_b^* \sim 2.91$ with a super-linear decay (inset), ensuring that the analysis at $N = 50$ is consistent with the thermodynamic limit. With respect to setups in higher dimensions, a 2D squared lattice with a side of N spins has a surface to volume ratio $4N/N^2 = 4/N$, while for a 3D cubic lattice the ratio is $6N^2/N^3 = 6/N$. Therefore, the 1D case we addressed with a ratio $1/N$ represents the most pronounced scenario. The ratio is of the same order independently of the dimension ($\sim N^{-1}$), suggesting that the same phenomenology should be observed in higher-dimensional setups.

Remarks.—We constructed a theoretical framework to characterize the evolution of a system coupled to the thermal bath only through its boundaries, presenting two complementary emblematic models with continuous and discrete d.o.f., respectively. While in the former a minimal intensity for the coupling is required, in the latter we proved how anomalous relaxation effects can survive arbitrary weak couplings. The proposed framework is general and applicable to any memoryless system exchanging heath with the thermal bath through limited d.o.f., including relaxations toward NESS [53]. Our results corroborate the validity of the ME as a nonequilibrium phenomenon, proving it is not an artifact due to full couplings. The existence of far from equilibrium relaxations in the weak coupling limit are yet another counterintuitive result related to the discreteness of the d.o.f. [54].

O. R. is supported by the Abramson Family Center for Young Scientists, the Israel Science Foundation Grant No. 950/19, and by the Minerva foundation. G. T. is supported by the Center for Statistical Mechanics at the Weizmann Institute of Science, Grant No. 662962 of the Simons Foundation, the grants HALT and Hydrotronics of the EU Horizon 2020 program, and the NSF-BSF Grant No. 2020765. We thank David Mukamel and Attilio L. Stella for useful discussions.

*oren.raz@weizmann.ac.il

[1] Z. Lu and O. Raz, Nonequilibrium thermodynamics of the Markovian Mpemba effect and its inverse, Proc. Natl. Acad. Sci. U.S.A. **114**, 5083 (2017).
[2] A. Gal and O. Raz, Precooling Strategy Allows Exponentially Faster Heating, Phys. Rev. Lett. **124**, 060602 (2020).
[3] A. Lapolla and A. c. v. Godec, Faster Uphill Relaxation in Thermodynamically Equidistant Temperature Quenches, Phys. Rev. Lett. **125**, 110602 (2020).
[4] A. Militaru, A. Lasanta, M. Frimmer, L. L. Bonilla, L. Novotny, and R. A. Rica, Kovacs Memory Effect with an Optically Levitated Nanoparticle, Phys. Rev. Lett. **127**, 130603 (2021).
[5] R. Holtzman and O. Raz, Landau theory for the Mpemba effect through phase transitions, Commun. Phys. **5**, 280 (2022).
[6] Aristotle, *Meteorology* (Harvard University Press, Cambridge, MA, 1962), Book I, Chap. XII, pp. 85–87.
[7] E. B. Mpemba and D. G. Osborne, Cool?, Phys. Educ. **4**, 172 (1969).
[8] M. Jeng, The Mpemba effect: When can hot water freeze faster than cold?, Am. J. Phys. **74**, 514 (2006).
[9] P. Chaddah, S. Dash, K. Kumar, and A. Banerjee, Overtaking while approaching equilibrium, arXiv:1011.3598.
[10] C. Hu, J. Li, S. Huang, H. Li, C. Luo, J. Chen, S. Jiang, and L. An, Conformation directed Mpemba effect on polylactide crystallization, Cryst. Growth Des. **18**, 5757 (2018).
[11] Y.-H. Ahn, H. Kang, D.-Y. Koh, and H. Lee, Experimental verifications of Mpemba-like behaviors of clathrate hydrates, Korean J. Chem. Eng. **33**, 1 (2016).
[12] A. Kumar and J. Bechhoefer, Exponentially faster cooling in a colloidal system, Nature (London) **584**, 64 (2020).
[13] A. Kumar, R. Chétrite, and J. Bechhoefer, Anomalous heating in a colloidal system, Proc. Natl. Acad. Sci. U.S.A. **119**, e2118484119 (2022).
[14] J. Bechhoefer, A. Kumar, and R. Chétrite, A fresh understanding of the Mpemba effect, Nat. Rev. Phys. **3**, 534 (2021).
[15] Y. Tao, W. Zou, J. Jia, W. Li, and D. Cremer, Different ways of hydrogen bonding in water—why does warm water freeze faster than cold water?, J. Chem. Theory Comput. **13**, 55 (2016).
[16] X. Zhang, Y. Huang, Z. Ma, Y. Zhou, J. Zhou, W. Zheng, Q. Jiang, and C. Q. Sun, Hydrogen-bond memory and water-skin supersolidity resolving the Mpemba paradox, Phys. Chem. Chem. Phys. **16**, 22995 (2014).
[17] M. Vynnycky and S. Kimura, Can natural convection alone explain the Mpemba effect?, Int. J. Heat Mass Transfer **80**, 243 (2015).
[18] D. Auerbach, Supercooling and the Mpemba effect: When hot water freezes quicker than cold, Am. J. Phys. **63**, 882 (1998).

[19] S. M. Mirabedin and F. Farhadi, Numerical investigation of solidification of single droplets with and without evaporation mechanism, Int. J. Refrig. **73**, 219 (2017).

[20] A. Gijón, A. Lasanta, and E. R. Hernández, Paths towards equilibrium in molecular systems: The case of water, Phys. Rev. E **100**, 032103 (2019).

[21] A. Lasanta, F. Vega Reyes, A. Prados, and A. Santos, When the Hotter Cools More Quickly: Mpemba Effect in Granular Fluids, Phys. Rev. Lett. **119**, 148001 (2017).

[22] A. Torrente, M. A. López-Castaño, A. Lasanta, F. V. Reyes, A. Prados, and A. Santos, Large Mpemba-like effect in a gas of inelastic rough hard spheres, Phys. Rev. E **99**, 060901(R) (2019).

[23] A. Biswas, V. V. Prasad, O. Raz, and R. Rajesh, Mpemba effect in driven granular Maxwell gases, Phys. Rev. E **102**, 012906 (2020).

[24] A. Santos and A. Prados, Mpemba effect in molecular gases under nonlinear drag, Phys. Fluids **32**, 072010 (2020).

[25] A. Biswas, V. V. Prasad, and R. Rajesh, Mpemba effect in anisotropically driven inelastic Maxwell gases, J. Stat. Phys. **186**, 45 (2022).

[26] A. Megías, A. Santos, and A. Prados, Thermal versus entropic Mpemba effect in molecular gases with nonlinear drag, Phys. Rev. E **105**, 054140 (2022).

[27] S. Takada, H. Hayakawa, and A. Santos, Mpemba effect in inertial suspensions, Phys. Rev. E **103**, 032901 (2021).

[28] R. Gómez González, N. Khalil, and V. Garzó, Mpemba-like effect in driven binary mixtures, Phys. Fluids **33**, 053301 (2021).

[29] R. G. González and V. Garzó, Non-monotonic Mpemba effect in binary molecular suspensions, in *EPJ Web of Conferences* (EDP Sciences, 2021), Vol. 249, p. 09005.

[30] E. Mompó, M. López-Castaño, A. Lasanta, F. Vega Reyes, and A. Torrente, Memory effects in a gas of viscoelastic particles, Phys. Fluids **33**, 062005 (2021).

[31] R. Chétrite, A. Kumar, and J. Bechhoefer, The metastable Mpemba effect corresponds to a non-monotonic temperature dependence of extractable work, Front. Phys. **9**, 141 (2021).

[32] M. R. Walker and M. Vucelja, Anomalous thermal relaxation of Langevin particles in a piecewise-constant potential, J. Stat. Mech. (2021) 113105.

[33] D. M. Busiello, D. Gupta, and A. Maritan, Inducing and optimizing Markovian Mpemba effect with stochastic reset, New J. Phys. **23**, 103012 (2021).

[34] F. J. Schwarzendahl and H. Löwen, Anomalous Cooling and Overcooling of Active Systems, Phys. Rev. Lett. **129**, 138002 (2022).

[35] F. Carollo, A. Lasanta, and I. Lesanovsky, Exponentially Accelerated Approach to Stationarity in Markovian Open Quantum Systems through the Mpemba Effect, Phys. Rev. Lett. **127**, 060401 (2021).

[36] M. Baity-Jesi, E. Calore, A. Cruz, L. A. Fernandez, J. M. Gil-Narvión, A. Gordillo-Guerrero, D. Iñiguez, A. Lasanta, A. Maiorano, E. Marinari *et al.*, The Mpemba effect in spin glasses is a persistent memory effect, Proc. Natl. Acad. Sci. U.S.A. **116**, 15350 (2019).

[37] A. Nava and M. Fabrizio, Lindblad dissipative dynamics in the presence of phase coexistence, Phys. Rev. B **100**, 125102 (2019).

[38] Z.-Y. Yang and J.-X. Hou, Non-Markovian Mpemba effect in mean-field systems, Phys. Rev. E **101**, 052106 (2020).

[39] N. Vadakkayil and S. K. Das, Should a hotter paramagnet transform quicker to a ferromagnet? Monte Carlo simulation results for Ising model, Phys. Chem. Chem. Phys. **23**, 11186 (2021).

[40] I. Klich, O. Raz, O. Hirschberg, and M. Vucelja, Mpemba Index and Anomalous Relaxation, Phys. Rev. X **9**, 021060 (2019).

[41] I. González-Adalid Pemartín, E. Mompó, A. Lasanta, V. Martín-Mayor, and J. Salas, Slow growth of magnetic domains helps fast evolution routes for out-of-equilibrium dynamics, Phys. Rev. E **104**, 044114 (2021).

[42] Z.-Y. Yang and J.-X. Hou, Mpemba effect of a mean-field system: The phase transition time, Phys. Rev. E **105**, 014119 (2022).

[43] R. Tehver, F. Toigo, J. Koplik, and J. R. Banavar, Thermal walls in computer simulations, Phys. Rev. E **57**, R17 (1998).

[44] D. Toton, C. D. Lorenz, N. Rompotis, N. Martsinovich, and L. Kantorovich, Temperature control in molecular dynamic simulations of non-equilibrium processes, J. Phys. Condens. Matter **22**, 074205 (2010).

[45] N. Van Kampen, Diffusion in inhomogeneous media, J. Phys. Chem. Solids **49**, 673 (1988).

[46] The specific normalization chosen for $\mathbf{W}^{\{\mathrm{BC,ST}\}}$ changes the value of C, but not its limiting cases. Specifically, we chose to normalize with respect to the maximum rate so that $\max(\mathbf{W}_{ij}^{\mathrm{ST}}) = \max(\mathbf{W}_{ij}^{\mathrm{BC}}) \equiv 1$.

[47] G. Teza and A. L. Stella, Exact Coarse Graining Preserves Entropy Production Out of Equilibrium, Phys. Rev. Lett. **125**, 110601 (2020).

[48] G. Teza, Out of equilibrium dynamics: From an entropy of the growth to the growth of entropy production, Ph. D. Thesis, University of Padova, 2020.

[49] R. J. Glauber, Time-dependent statistics of the Ising model, J. Math. Phys. **4**, 294 (1963).

[50] B. U. Felderhof, Spin relaxation of the Ising chain, Rep. Math. Phys. **1**, 215 (1971).

[51] R. W. Hamming, Error detecting and error correcting codes, Bell Syst. Tech. J. **29**, 147 (1950).

[52] A. Bookstein, V. A. Kulyukin, and T. Raita, Generalized hamming distance, Inf. Retr. **5**, 353 (2002).

[53] See Supplemental Material at http://link.aps.org/supplemental/10.1103/PhysRevLett.131.017101 for additional details of the calculations at the basis of the results presented in the main text.

[54] G. Teza, R. Yaacoby, and O. Raz, Far from equilibrium relaxation in the weak coupling limit, arXiv:2203.11644.

[55] S. Katz, J. L. Lebowitz, and H. Spohn, Phase transitions in stationary nonequilibrium states of model lattice systems, Phys. Rev. B **28**, 1655 (1983).

[56] G. Teza, S. Iubini, M. Baiesi, A. L. Stella, and C. Vanderzande, Rate dependence of current and fluctuations in jump models with negative differential mobility, Physica (Amsterdam) **552A**, 123176 (2020), tributes of non-equilibrium statistical physics.

[57] G. Teza, R. Yaacoby, and O. Raz, Eigenvalue Crossing as a Phase Transition in Relaxation Dynamics, Phys. Rev. Lett. **130**, 207103 (2023).

[58] A. L. Stella, A. Chechkin, and G. Teza, Anomalous Dynamical Scaling Determines Universal Critical Singularities, Phys. Rev. Lett. **130**, 207104 (2023).

[59] A. L. Stella, A. Chechkin, and G. Teza, Universal singularities of anomalous diffusion in the Richardson class, Phys. Rev. E **107**, 054118 (2023).

[60] J. Meibohm and M. Esposito, Finite-Time Dynamical Phase Transition in Nonequilibrium Relaxation, Phys. Rev. Lett. **128**, 110603 (2022).

[61] G. Teza, S. Suweis, M. Gherardi, A. Maritan, and M. Cosentino Lagomarsino, Network model of conviction-driven social segregation, Phys. Rev. E **99**, 032310 (2019).